A model for generating synthetic blood pressure waveform

Adam Mahdi, Gari D. Clifford, and Stephen J. Payne

***Abstract*—*Objective:* A new model capable of simulating many important aspects of human arterial blood pressure (ABP) is proposed. *Methods:* Both data-driven approach and physiological principles have been applied to describe the time series of diastolic, systolic, dicrotic notch and dicrotic peak pressure points. *Results:* Major static and dynamic features of the model can be prescribed by the user, including heart rate, mean systolic and diastolic pressure, and the corresponding physiological control quantities, such as baroreflex sensitivity coefficient and Windkessel time constant. *Conclusion:* A realistic ABP generator can be used to compile a virtual database of signals reflecting individuals with different clinical conditions and signals containing common artefacts. *Significance:* The ABP model permits to create a platform to assess a wide range of biomedical signal processing approaches and be used in conjunction with, e.g., Kalman filters to improve the quality of ABP signals.**

***Index Terms*—Synthetic ABP, systolic pressure, diastolic pressure, baroreflex, heart rate variability**

I. Introduction

ARTERIAL blood pressure (ABP) is one of the most routinely used physiological signals in the assessment of cardiovascular diseases. It is the result of an interaction between the heart and arterial system. Thus the shape of the ABP waveform (see Fig. 1) is a consequence of the changes in aortic input impedance and modifications in cardiac function [15].

Currently, many biomedical approaches use either a complete ABP signal or some of its features, most commonly diastolic and systolic pressure points. The latter can be extracted by robust signal processing techniques and used along other signals to provide estimates for a variety of physiological benchmarks, e.g. baroreflex sensitivity [23] and cerebral autoregulation index [17], [18]. A realistic synthetic ABP generator could provide an intermediate framework for examining those computational methods. In a controlled environment it would be possible to test, even to quantify the influence of different noise levels and sampling frequencies present in the data [9].

In this paper a new physiology-based, data-driven ABP model capable of generating many known characteristics of human blood pressure waveforms is proposed. A number of static and dynamic features of the model can be defined by the user *a priori*, including heart rate, mean systolic and diastolic pressure, and the corresponding control quantities such as baroreflex senstivity coefficient [4] and Windkessel time constant [24]. The paper illustrates how the model can be used to create an artificial database of ABP signals reflecting individuals with different ABP characteristics, including waveforms containing both common artefacts and regular features such as ectopic heartbeats.

The anonymized ABP data, used in this work, were measured noninvasively during a sit-to-stand manoeuvere using a photoplethysmographic Finapres monitor (Ohmeda Monitoring Systems, Englewood, CO). The subject's nondominant hand was supported by a sling at the level of the right atrium to eliminate hydrostatic pressure effects. The preparation and recording methods have been described in detail in [10].

The paper is organized as follows. Section II provides background information on short-term ABP regulation and describes the main features of ABP. Section III introduces the ABP model and includes the derivation of its components. The results and simulations are presented in Section IV. Finally the discussion of the model together with some possible extensions of it are included in Section V.

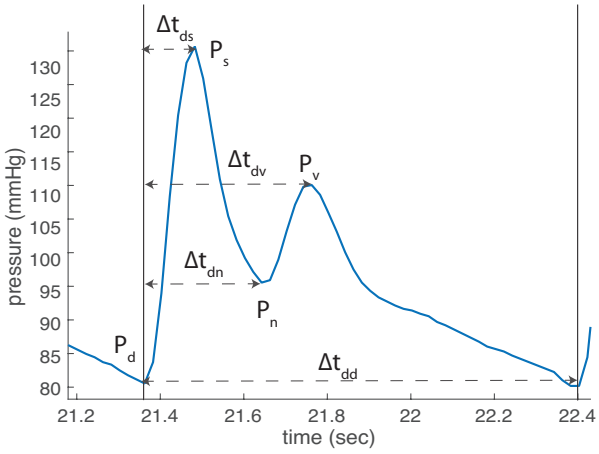

Fig. 1. An example of aortic blood pressure morphology during one cardiac cycle with indicated diastolic $\mathrm{P_d}$, systolic $\mathrm{P_s}$ and dicrotic notch $\mathrm{P_n}$ and dicrotic peak $\mathrm{P_v}$. Moreover, Δt_{ds} Δt_{dn} and Δt_{dv} denote the time intervals between the onset of ABP and the diastolic, dicrotic notch and dicrotic peak, respectively. Finally Δt_{dd} is the period of the cardiac cycle defined as the time between two consecutive diastolic pressure points.

II. ABP regulation

The primary role of the blood pressure is to provide the driving force for blood flow to circulate in the vast network of

A Mahdi and SJ Payne: Institute of Biomedical Engineering, Department of Engineering Science, University of Oxford, Oxford, UK. Emails: adam.mahdi@eng.ox.ac.uk (A Mahdi), SJ Payne: stephen.payne@keble.ox.ac.uk (SJ Payne)

Gari D. Clifford: Departments of Biomedical Informatics & Biomedical Engineering, Emory University & Georgia Institute of Technology, Atlanta, GA, USA

blood vessels to supply adequate oxygenation, nutrient delivery, waste removal and perform other physiological functions.

It is believed that the main short term contributor to the blood pressure control system is the baroreflex (or baroreceptor reflex), a negative feedback system which uses specialized neurons called baroreceptors for signaling [6]. The baroreceptor neurons are stretch receptors, located in the aortic arch and carotid sinuses, which terminate in the central nervous system. Thus information is transmitted from the baroreceptors to the central nervous system, where it is integrated, and sent further via the slow sympathetic and fast parasympathetic pathways. This leads to the release or inhibition of neurotransmitters which modulate, among other things, the heart rate (or equivalently the length of the cardiac cycle).

Beat-to-beat changes in blood pressure and heart rate in resting humans are mainly due to respiration. Respiratory sinus arrhythmia (RSA) is a phenomenon consisting of heart rate variability in synchrony with respiration, manifesting itself by the period of the cardiac cycle being shortened during inspiration and prolonged during expiration [25]. The RSA oscillation can be seen in a high frequency band of the power spectrum as a peak in the frequency range around $0.15 - 0.35\,\mathrm{Hz}$. There is also a second peak in the power spectrum corresponding to a much lower frequency of about $0.1\,\mathrm{Hz}$ [10]. Although the exact origin of those $10\,\mathrm{sec}$ slow rhythms, called Mayer waves, is still under debate, it is thought to be due to the delay in the sympathetic feedback loop of the baroreflex [5].

Changes in ABP are mainly due to the pumping action of the heart and its various stages are closely linked with the ABP morphology. The four main features of ABP, namely diastolic, systolic, dicrotic notch and dicrotic peak points, will be modelled and discussed both here and in the following sections.

Diastolic pressure $(\mathrm{t_d^j}, \mathrm{P_d^j})$: At the end of the isovolumic contraction phase, i.e. just before the opening of the aortic valve, ABP is at its low value, called the diastolic pressure and denoted here by P_d^j, for jth cardiac cycle. Let $\Delta t_{dd}^j = t_d^{j+1} - t_d^j$ be the time interval between the occurrence of two consecutive diastolic values P_d^j and P_d^{j+1}, respectively. The time series of the diastolic time points can be written as:

$$t_d^{j+1} = t_d^j + \Delta t_{dd}^j, \tag{1}$$

where $j = 1, \ldots, N$, and $N \in \mathbb{N}$ is the number of cardiac cycles. It is assumed that the jth cardiac cycle begins at the time occurrence of P_d^{j+1}; and in the full N cardiac cycles, there are $N+1$ diastolic points.

Systolic pressure $(\mathrm{t_s^j}, \mathrm{P_s^j})$: The beginning of systole is marked by the closure of the atrioventricular valve and the beginning of the ventricular contraction. Following isovolumic contraction the aortic valve opens and the arterial pressure rises, reaching its peak P_s^j, called the systolic pressure. Let $\Delta t_{ds}^j = t_d^j - t_s^j$ be the time interval between the occurrence of diastolic P_d^j and systolic pressure P_s^j within the jth cycle. The time series of systolic time points can be written as:

$$t_s^j = t_d^j + \Delta t_{ds}^j. \tag{2}$$

Dicrotic notch $(\mathrm{t_n^j}, \mathrm{P_n^j})$: During the ejection phase initiated by the opening of the aortic valve the arterial ABP increases reaching its peak at the systolic pressure, and then decreases until the beginning of the isovolumic relaxation indicated by the closure of the aortic valve. This marks the onset of the secondary peak, called the dicrotic notch P_n^j, which is characterized by a brief increase of ABP. Let $\Delta t_{dn}^j = t_d^j - t_n^j$ be the time interval between the occurrence of diastolic P_d^j and dicrotic notch P_n^j pressure. The time series of dicrotic notch time points can be expressed as:

$$t_n^j = t_d^j + \Delta t_{dn}^j. \tag{3}$$

Dicrotic peak $(\mathrm{t_v^j}, \mathrm{P_v^j})$: The increase of the ABP following the onset of the dicrotic notch lasts until reaching some value $\mathrm{P_v^j}$, called the dicrotic peak, followed by a gradual decline until reaching the next diastolic pressure $\mathrm{P_d^j}$. Let $\Delta t_{dv}^j = t_d^j - t_v^j$ be the time interval between the occurrence of diastolic pressure and dicrotic peak. The time series of the dicrotic peaks time points can be written as:

$$t_v^j = t_d^j + \Delta t_{dv}^j. \tag{4}$$

III. ABP MODEL

The ABP model is developed in three stages: first, a general modelling framework is proposed; then the time series (1)-(4) are generated via a data-driven approach; and finally the corresponding time series of pressure values are described using physiological principles. Related modelling approaches for ECG were proposed in [14], [20], [21], [16].

Model framework. Consider a function $\mathrm{BP}^j(t)$, which is an approximation of the jth cardiac cycle waveform. In general, it can be modelled as

$$\mathrm{BP}^j(t) = \begin{cases} f_{ds}^j(t) & t \in [t_d^j,\, t_s^j] \\ f_{sn}^j(t) & t \in [t_s^j,\, t_n^j] \\ f_{nv}^j(t) & t \in [t_n^j,\, t_v^j] \\ f_{vd}^j(t) & t \in [t_v^j,\, t_d^{j+1}] \end{cases} \tag{5}$$

where each of the components $f_{ds}^j(t)$, $f_{sn}^j(t)$, $f_{nv}^j(t)$ and $f_{vd}^j(t)$ describe the portion of ABP in the corresponding interval indicated in (5) [see Sec. II]. There are many reasonable choices for modelling the components in (5). In order to reflect the two time-scale decay of the blood pressure [c.f. Fig. 1] during the diastole, a piecewise-smooth approach is proposed, see (15) in the Appendix.

The synthetic ABP is generated by combining N pressure waveforms:

$$\mathrm{BP}(t) = \left\{\mathrm{BP}^1(t), \mathrm{BP}^2(t), \ldots, \mathrm{BP}^N(t)\right\} \tag{6}$$

where $\mathrm{BP}^j(t)$ is defined in (5). The time series

$$\{(t_d^j, P_d^j), (t_s^j, P_s^j), (t_n^j, P_n^j), (t_v^j, P_v^j)\}, \qquad j = 1, \ldots, N, \tag{7}$$

are the characteristic features (onsets and peaks) of the ABP and are needed to generate each waveform (5) of the cardiac cycle. Since the extraction of time series (7) is common practice in biomedical signal processing, the synthetic ABP can be easily compared to the real ABP signal.

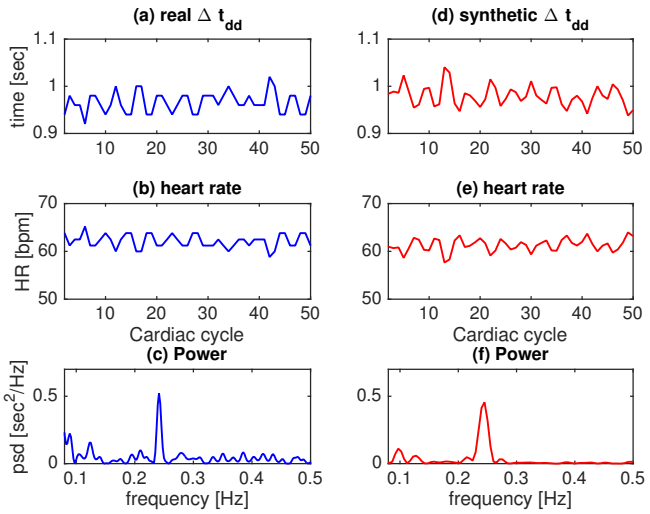

Fig. 2. Features of the ABP time series including cardiac cycle, heart rate and its power spectrum for an elderly normotensive individual (left column (a)-(c)) and the synthetic data generated by the model (right column (d)-(f)). Note that the power spectral density plots show visible Mayer waves in the low frequency band $(0.05-0.15)$ and RSA waves in the high frequency band $(0.15-0.5)$.

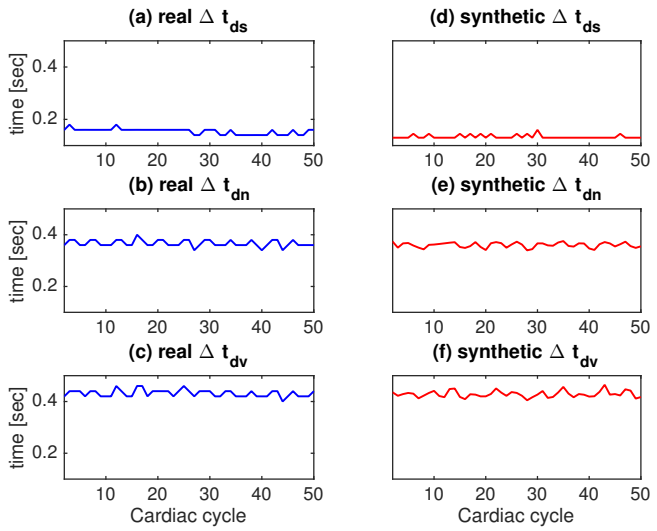

Fig. 3. Time-series of the differences between the occurrence of diastolic pressure the rest of the peaks of the ABP waveform.

Modelling ABP time points. The time series of differences between the onset of ABP and the occurrence of the next diastolic, dicrotic notch, dicrotic peak and the following onset of ABP, that is,

$$\Delta t_k^j, \qquad k \in \{dd,\, ds,\, dn,\, dv\}, \tag{8}$$

can be used to calculate t_d^j, t_s^j, t_n^j and t_v^j with the help of expressions (1)-(4). A data-driven approach to the generation of (8) is presented below.

The value Δt_{dd}^j is the period of the jth cardiac cycle from which the instantaneous heart rate can simply be obtained as

$$\mathrm{HR}^j = 60/\Delta t_{dd}^j. \tag{9}$$

The incorporation of the realistic heart rate variability, in particular RSA and Mayer waves with the characteristic peaks in the power spectrum at around $0.25\,\mathrm{Hz}$ and $0.1\,\mathrm{Hz}$ respectively, will now be considered. Fig. 2(a-c) show a typical plot of cardiac cycles, the corresponding instantaneous heart rate and the power spectrum density (PSD), with visible peaks in the low frequency (0.04 to $0.15\,\mathrm{Hz}$) high frequency (0.15 to $0.40\,\mathrm{Hz}$) bands (see Sec. II). By plotting PSD for Δt_{ds}^j, Δt_{dn}^j, Δt_{dv}^j and Δt_{dd}^j extracted from different ABP signals, we observed that they exhibit similar spectral content. Thus the incorporation of Mayer and RSA waves into the time series (8) is accomplished by the following unified approach:

$$\Delta t_k^j = \Delta \bar{t}_k + \alpha_k \Big[c_m \sin(2\pi f_M\, j) + c_R \sin(2\pi f_R\, j) \Big] + \epsilon_k\, \mathcal{E}_k^j, \tag{10}$$

where $\Delta \bar{t}_k$ denotes the mean value of the signal, $\mathcal{E}_k^j$ is a random variable for additive noise, α_k and ϵ_k are the scaling constants corresponding to the periodic and noise components, respectively; γ_M, γ_R are the amplitudes; and f_M, f_R are the frequencies (in Hz) of the Mayer and RSA waves, respectively.

Modelling ABP pressure points. Here we model the time series of pressure values P_d^j, P_s^j, P_n^j and P_v^j, corresponding to the time occurrences of those events at t_d^j, t_s^j, t_n^j and t_v^j using well established physiological principles.

The fast parasympathetic (vagal) branch of the autonomic control system exerts beat-to-beat effects on each period of the cardiac cycle and therefore on the instantaneous heart rate (see (9)). The first approximation of the action of the baroreflex [3], [4], [13] on the cardiac pacemaker can be described as $\Delta t_{dd}^j = \alpha_0 P_s^j + c_1$, where α_0 is the baroreflex sensitivity coefficient [23], [19], and c_1 is the offset. We immediately obtain the values for the systolic pressure $P_s^j = (\Delta t_{dd}^j - c_1)/\alpha_0$. However, it might be more convenient to express the offset c_1 in function of the more intuitive mean systolic pressure $\overline{P}_s$ as $P_s^j = \overline{P}_s + (\Delta t_{dd}^j - \Delta \bar{t}_{dd})/\alpha_0$. Thus the relationship between the cardiac cycles and the systolic pressure with added noise [23], [4] is

$$P_s^j = \overline{P}_s + (\Delta t_{dd}^j - \Delta \bar{t}_{dd})/\alpha_0 + \gamma_s\, \mathcal{G}_s^j, \tag{11}$$

where $\mathcal{G}_s^j$ is the random variable and γ_s is the scaling factor.

Let $P_d^j = \overline{P}_d + p_d^j$ and $P_s^j = \overline{P}_s + p_s^j$, where p_d^j and p_s^j are the variations around the mean value of the diastolic $\overline{P}_d$ and systolic $\overline{P}_s$ pressure, respectively. By the application of the Windkessel model [24] and an approximation derived in [4] we obtain $p_d^j = \overline{P}_d \cdot p_s^{j-k} \cdot (1/\overline{P}_s - \alpha_0/\tau)$. Thus the systolic pressure points are

$$P_d^j = \overline{P}_d + \overline{P}_d \Big[p_s^{j-k} \cdot (1/\overline{P}_s - \alpha_0/\tau) \Big], \tag{12}$$

where τ is the Windkessel time constant.

There is an approximately linear relationship between the pulse pressure $\Delta P_{ds}^j = P_s^j - P_d^j$ and $\Delta P_{dn}^j = P_n^j - P_d^j$. For dicrotic notch pressure, it can be formally written as $\Delta P_{dn}^j \approx a_n\, \Delta P_{ds}^j - b_n$, where a_n and b_n are the scaling factor and the shift. An analogous approximate equality holds for the dicrotic peak, where the scaling and the shift factors are now a_v and b_v, respectively. We confirmed that this

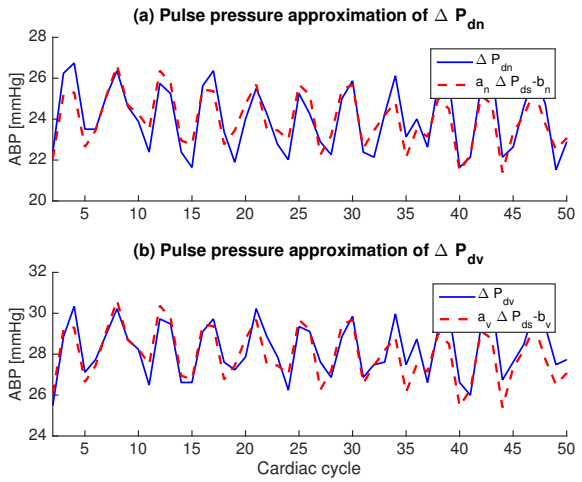

Fig. 4. Approximately linear relationship between the pulse pressure ΔP^j_{ds} and (a) ΔP^j_{dn} and (b) ΔP^j_{dv}. The constants used in the simulation are $(a_n, b_n) = (0.5, 8)$ and $(a_v, b_v) = (0.5, 12)$.

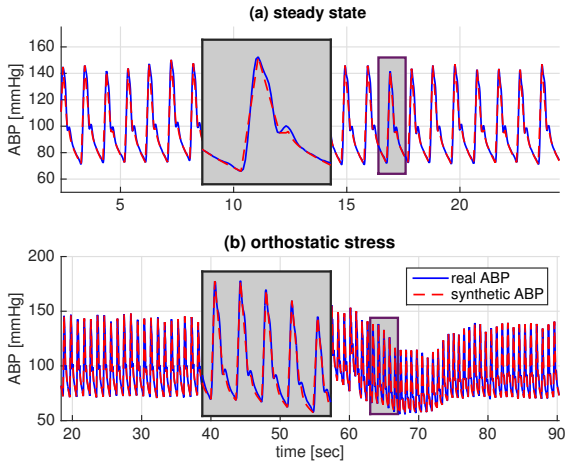

Fig. 5. Beat-to-beat fit of the synthetic ABP (red broken) waveform to the real ABP (blue solid) from an elderly normotensive individual. (a) Comparison of the two signals during steady-state period (sitting phase) and (b) during orthostatic stress (sit-to-stand manoeuvre).

relationship holds for most of the time-series extracted from the steady-state portion of ABP measured in young and elderly individuals (see an example in Fig. 4). Thus we calculate the dicrotic notch pressure points as

$$P^j_n = P^j_d + \Delta P^j_{dn} \approx P^j_d + a_n \, \Delta P^j_{ds} - b_n. \qquad (13)$$

As before, there is an approximate expression $\Delta P^j_{dv} \approx a_v \, \Delta P^j_{ds} - b_v$, which can be used to obtain

$$P^j_v = P^j_d + \Delta P^j_{dv} \approx P^j_d + a_v \, \Delta P^j_{ds} - b_v, \qquad (14)$$

where again a_v and b_v are the scaling factor and the shift associated with the dicrotic peak.

IV. Results

The results featured here are intended to show the new ABP model's capabilities to generate realistic ABP signals including common ABP artefacts.

The ABP model parameters used here to generate the synthetic blood pressure signal are given in Table I (time points) and Table II (pressure points). The values have been chosen to match real ABP data [blue solid line in Figs 2-5], which was taken from an elderly normotensive individual performing a sit-to-stand manoeuvre.

Fig. 2 shows the real and synthetically generated time series of cardiac cycles Δt^j_{dd} [Figs. 2(a,d)] together with the corresponding instantaneous heart rate HR^j [Figs. 2(b,e)]. The PSD [Figs. 2(c,f)] display visible Mayer waves in the low frequency band $(0.05 - 0.15)$ and RSA waves in the high frequency band $(0.15 - 0.5)$. The Lomb-Scargle periodogram [11], [22], [8] for unevenly sampled time series was used to estimate the power spectrum.

The time intervals Δt^j_k in (8) are modelled here using a data-driven approach described by equation (10). A binomially distributed additive noise $\mathcal{E}_{dd} \sim \mathcal{B}(N, \pi_s)$, where N is the number of trials of the Bernoulli process with probability of success π_s, has been added to each time series for a purely empirical rationale. As a result [Figs. 3(d-f)] synthetically generated time series Δt^j_{ds}, Δt^j_{ds}, Δt^j_{ds} exhibit qualitatively equivalent fluctuations as the ones extracted from the real ABP signal [Figs. 3(a-c)]. In general Δt^j_{ds} is nearly constant, with randomly and sparsely distributed deviation "spikes". Thus the periodic coefficient α_{ds} is set to zero here [see Tab. I].

The linear relationship between ΔP^j_{dn}, ΔP^j_{dn} and the pulse pressure ΔP^j_{ds} (see (13) and (14)) is illustrated in Fig. 4. The dicrotic notch scaling-shift pair $(a_n, b_n) = (0.5, 8)$ has been estimated by fitting $a_n \, \Delta P^j_{ds} - b_n$ to ΔP^j_{dn} to the real ABP signal [Fig. 4(a)]. The pair $(a_v, b_v) = (0.5, 12)$ [Fig. 4(b)] is calculated similarly. Recall that the time series ΔP^j_{dn}, ΔP^j_{dv} are used to compute the dicrotic notch P^j_n and dicrotic peak P^j_v pressure points, respectively.

The piecewise smooth approach (15), aimed to approximate an ABP waveform, is illustrated in Fig. 5. Beat-to-beat fit of the model to the steady-state portion of ABP is shown in Fig. 5(a). A plot of ABP during a single cardiac cycle, with the visible two time-scale decrease of blood pressure, is shown in the magnifying window. Qualitatively similar results are obtained for a non-steady-state ABP signal [Fig. 5(b)], here due to orthostatic stress induced by sit-to-stand manoeuvre. The plots have been produced by extracting the time series (7) from the real ABP signal *a priori*, by applying a peak detection algorithm, and then used as input for the ABP model (6).

Some of the capabilities of the new ABP model are illustrated in Fig. 6. The blood pressure generated for different values of the mean arterial pressure (MAP) are shown in Fig. 6 (a,b). Recall that MAP is calculated as $\mathrm{MAP} = \overline{P}_d + (\overline{P}_s - \overline{P}_d)$, where $\overline{P}_d$ and $\overline{P}_s$ are the mean diastolic and mean systolic pressure, respectively. The ABP signal generated for HR=40 and HR=90 is given in Fig. 6 (c,d). The mean values of heart rate can be expressed in terms of the mean cardiac cycle $\Delta \overline{t}_{dd}$ via relationship (9). Finally, the synthetic ABP generated for the baroreflex sensitivity $\alpha_0 = 5$ and $\alpha_0 = 15$ is shown in Fig. 6 (e,f).

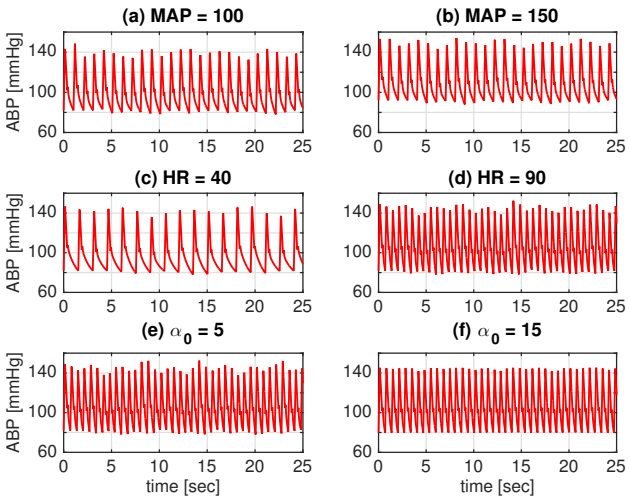

Fig. 6. Synthetic ABP generated by the model for the indicated values of: (a,b) mean arterial pressure MAP; (c,d) heart rate HR; (e,f) baroreflex sensitivity α_0. Unless it has been indicated explicitly, the generic values of the parameters of the model used here are given in Tables I and II.

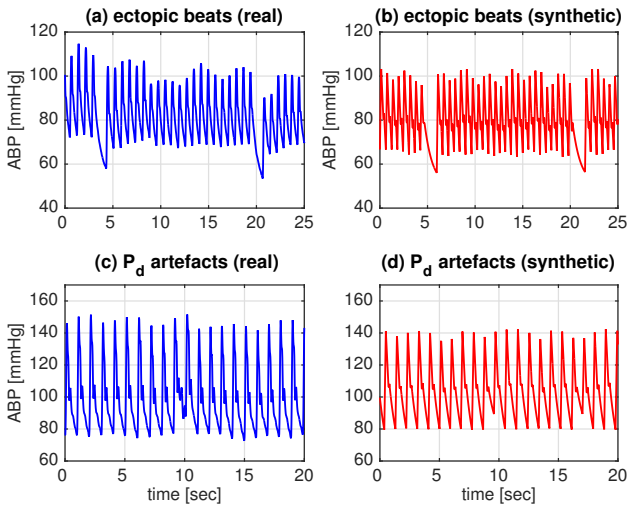

Fig. 7. Real and synthetic ABP with ectopic beats (a,b) and diastolic artefacts (c,d).

The model is also capable of generating ABP with additional features randomly distributed in the signal, including various types of artefacts. The reflection of ectopic heartbeats in the real blood pressure [Fig. 7(a)] is characterized by the extended drop of ABP. Similar effects can be obtained by the ABP generator [Fig. 7(b)]. The real and synthetic ABP with events affecting diastolic values of the individual cardiac cycles are shown in Fig. 7(c,d).

V. Discussion

The ABP model, introduced here, is capable of simulating many important aspects of human blood pressure. The spectral content of the time series of periods (of cardiac cycles) can be selected by the user in advance [see (10)]. A number of other dynamic features of the ABP model can also be prescribed by changing its basic parameters [Table II]. This includes mean systolic $\overline{P}_s$ and diastolic pressure $\overline{P}_d$, and the corresponding physiological control quantities, namely baroreflex senstivity coefficient α_0 and Windkessel time constant τ, respectively.

There are numerous advantages of having a realistic ABP generator. It can, for example, serve as a tool to compile a virtual database of blood pressure waveforms reflecting individuals under different clinical conditions. This can be used as a platform for testing different biomedical signal processing approaches (e.g. in the context of cerebral autoregulation [17], [12]). Additional tests can be performed for various types and levels of noise and sampling frequencies, which is an important step in the validation process.

A limited application of the new model in compiling a virtual ABP database is shown in Figs. 6, where regular (i.e. artefacts-free) signals with different values of the mean arterial pressure, heart rate and baroreflex sensitivity is plotted. The database can easily be extended to include waveforms for the desired values of diastolic pressure (12), systolic pressure (11), dicrotic notch [see (13), (14)], signal morphology [see (15)] and noise levels [see (10)]. It is also possible to incorporate into the synthetic ABP certain artefacts often encountered in the real signal. An example of ectopic heartbeats and the corruption of a single diastolic pressure point have been illustrated in Fig. 7. However, many types of artefacts can also be easily simulated in a similar manner [9].

Generators of physiological signals, including ECG and ABP, have often been used in conjunction with Kalman filters in order to track the "true" signal and limit the contribution of noise [21], [20]. Typically this required the initial calibration of the model by fitting it to the real physiological data [2]. In the approach presented here the initial calibration is reduced to finding only five data points. Due to the specific design of the current ABP model, the filtering can be easily decoupled into separate components responsible for each of the characteristic features of the ABP (see (7)). This could permit the removal of certain artefacts embedded in the signal such as the corruption of a single peak, which typically cannot be detected by adaptive segmentation methods [7]. Kalman filter-based methods associated, for example, only with systolic time series can be used to correct this particular pressure point.

A limitation of the model is that equation (11) implies that the phase between the cardiac cycles periods t_{dd}^j and systolic pressure P_s is zero. It has previously been observed [4] that this is approximately the case in the region of the respiratory frequency around $(0.20 - 0.35\,\mathrm{Hz})$. However, close to $0.1\,\mathrm{Hz}$ the pressure leads the cardiac cycle periods by a substantial amount (approximately $\pi/3$ radians, [4]). Thus equation (11) cannot reflect the real data in the whole relevant physiological frequency range.

VI. Conclusion

A new model capable of generating realistic ABP waveforms is proposed here. In future work the authors plan to use it for compiling synthetic databases of blood pressure signals reflecting individuals under different conditions in order to test biomedical signal processing techniques applied in the context

k	dd	ds	dn	dv
$\Delta\bar{t}_k$	0.97	0.13	0.36	0.421
α_k	1.1	0	0.6	0.6
ϵ_k	0.015	0.015	0.005	0.007
$\mathcal{E}_k$	$\mathcal{B}(10, 0.07)$	$\mathcal{B}(10, 0.015)$	$\mathcal{B}(10, 0.1)$	$\mathcal{B}(10, 0.1)$

TABLE I
MODEL PARAMETERS TO GENERATE Δt_k^j, $k \in \{dd, ds, do, dv\}$.

Description	Symbol	Value	Units
Mean systolic pres.	$\overline{P}_s$	145.7	mmHg
Baroreflex sens.	α_0	7	ms/mmHg
Systolic noise	$[\gamma_s, \mathcal{G}_s^j]$	$[10, \mathcal{U}(0,1)]$	[-, mmHg]
Mean diastolic pres.	$\overline{P}_d$	69	mmHg
Windkessel const.	τ	1850	ms
Dicrotic notch pair	$[a_n, b_n]$	[0.5, 12]	[-, mmHg]
Dicrotic peak pair	$[a_v, b_v]$	[0.5, 8]	[-, mmHg]

TABLE II
MODEL PARAMETERS TO GENERATE P_k, $k \in \{d, s, n, v\}$.

of ABP and cerebral autoregulation [1]. It is also hoped that the model will be helpful when coupled it with filtering tools and artefact removal techniques.

APPENDIX A

The piecewise-smooth approach is proposed here to model the blood pressure waveform (5) as follows:

$$\begin{aligned} f_{ds}(t) &= (P_s - P_d)/(t_s - t_d) \cdot (t - t_d) + P_d \\ f_{sn}(t) &= (P_n - P_s)/(t_n - t_s) \cdot t + P_s - (P_n - P_s)/(t_n - t_s) t_s \\ f_{nv}(t) &= (P_v - P_n)/(t_v - t_n) \cdot t + P_n - (P_v - P_n)/(t_v - t_n) t_n \\ f_{vd}(t) &= P_{d'} + (P_v - P_{d'}) \cdot [(t_{d'} - t)/(t_{d'} - t_v)] \cdot F(t), \end{aligned} \tag{15}$$

where the function $F(t)$ is chosen so that the pressure during the last phase of diastole (i.e. in $[t_v, t_{d'}]$) exhibits a two time-scale decay. For convenience the superscript indicating the jth cardiac cycle has been omitted, and $t_{d'}$ denotes the end of the cardiac cycle (equivalently the beginning of the next cardiac cycle). The function $F(t)$ is modelled as

$$F(t) = c_d \exp[m_1(t_{d'} - t_v)] + (1 - c_d) \exp[m_2(t_{d'} - t_v)],$$

where $c_d \in [0, 1]$ and $m_1, m_2 \in \{1, \ldots, 10\}$ are the parameters shaping the decay function. Here $c_d = 0.5$, $m_1 = 1$ and $m_2 = 3$. Note that $F(t_v) = 1$ and thus $f_{pd'}(t_v) = P_v$ and $f_{pd'}(t_{d'}) = P_{d'}$.

ACKNOWLEDGEMENT

The authors acknowledge the support of EPSRC project EP/K036157/1. The authors thank Dr Lewis Lipsitz at the Hebrew SeniorLife (Boston, MA) for the access to anonymized ABP dataset.

REFERENCES

[1] N Angarita-Jaimes, H Kouchakpour, Jia Liu, RB Panerai, and DM Simpson. Optimising the assessment of cerebral autoregulation from black box models. *Medical Engineering & Physics*, 36(5):607–612, 2014.

[2] GD Clifford, A Shoeb, PE McSharry, and BA Janz. Model-based filtering, compression and classification of the ECG. *International Journal of Bioelectromagnetism*, 7(1):158–161, 2005.

[3] RW De Boer, JM Karemaker, and J Strackee. Relationships between short-term blood-pressure fluctuations and heart-rate variability in resting subjects I: a spectral analysis approach. *Medical and Biological Engineering and Computing*, 23(4):352–358, 1985.

[4] RW De Boer, JM Karemaker, and J Strackee. Relationships between short-term blood-pressure fluctuations and heart-rate variability in resting subjects II: a simple model. *Medical and Biological Engineering and Computing*, 23(4):359–364, 1985.

[5] RW DeBoer, JM Karemaker, and J Strackee. Hemodynamic fluctuations and baroreflex sensitivity in humans: a beat-to-beat model. *American Journal of Physiology-Heart and Circulatory Physiology*, 253(3):H680–H689, 1987.

[6] AC Guyton and JE Hall. *Guyton and Hall Textbook of Medical Physiology (11th ed.)*. Elsevier Saunders., Philadelphia, 2006.

[7] W Karlen, JM Ansermino, and G Dumont. Adaptive pulse segmentation and artifact detection in photoplethysmography for mobile applications. In *Conference proceedings: Annual International Conference of the IEEE Engineering in Medicine and Biology Society. IEEE Engineering in Medicine and Biology Society. Conference*, volume 2012, pages 3131–3134, 2011.

[8] P Laguna, GB Moody, and RG Mark. Power spectral density of unevenly sampled data by least-square analysis: performance and application to heart rate signals. *Biomedical Engineering, IEEE Transactions on*, 45(6):698–715, 1998.

[9] Q Li, RG Mark, and GD Clifford. Artificial arterial blood pressure artifact models and an evaluation of a robust blood pressure and heart rate estimator. *Biomedical Engineering OnLine*, 8(1):13, 2009.

[10] LA Lipsitz, S Mukai, J Hamner, M Gagnon, and V Babikian. Dynamic regulation of middle cerebral artery blood flow velocity in aging and hypertension. *Stroke*, 31:1897–1903, 2000.

[11] NR Lomb. Least-squares frequency analysis of unequally spaced data. *Astrophysics and Space Science*, 39(2):447–462, 1976.

[12] G Mader, MS Olufsen, and A Mahdi. Modeling cerebral blood flow velocity during orthostatic stress. *Annals of Biomedical Engineering*, 43:1748–1758, 2015.

[13] A Mahdi, J Sturdy, TJ Ottesen, and M Olufsen. Modeling the afferent dynamics of the baroreflex control system. *PLoS Computational Biology*, 9:e10033384, 2013.

[14] PE McSharry, GD Clifford, L Tarassenko, and L Smith. A dynamical model for generating synthetic electrocardiogram signals. *Biomedical Engineering, IEEE Transactions on*, 50(3):289–294, 2003.

[15] Y Nakayama, K Tsumura, N Yamashita, K Yoshimaru, and T Hayashi. Pulsatility of ascending aortic pressure waveform is a powerful predictor of restenosis after percutaneous transluminal coronary angioplasty. *Circulation*, 101(5):470–472, 2000.

[16] J Oster, J Behar, O Sayadi, S Nemati, A Johnson, and G Clifford. Semi-supervised ECG ventricular beat classification with novelty detection based on switching Kalman filters. *Biomedical Engineering, IEEE Transactions on*, 62(9), 2015.

[17] RB Panerai. Cerebral autoregulation: from models to clinical applications. *Cardiovasc Eng.*, 8:43–59, 2008.

[18] T Peng, AB Rowley, PN Ainslie, MJ Poulin, and SJ Payne. Multivariate system identification for cerebral autoregulation. *Annals of Biomedical Engineering*, 36(2):308–320, 2008.

[19] TG Pickering, B Gribbin, E Strange Petersen, DJC Cunningham, and P Sleight. Effects of autonomic blockade on the baroreflex in man at rest and during exercise. *Circulation research*, 30(2):177–185, 1972.

[20] R Sameni, MB Shamsollahi, C Jutten, and GD Clifford. A nonlinear Bayesian filtering framework for ECG denoising. *Biomedical Engineering, IEEE Transactions on*, 54(12):2172–2185, 2007.

[21] O Sayadi and MB Shamsollahi. ECG denoising and compression using a modified extended Kalman filter structure. *Biomedical Engineering, IEEE Transactions on*, 55(9):2240–2248, 2008.

[22] JD Scargle. Studies in astronomical time series analysis. II-statistical aspects of spectral analysis of unevenly spaced data. *The Astrophysical Journal*, 263:835–853, 1982.

[23] HS Smyth, P Sleight, and GW Pickering. Reflex regulation of arterial pressure during sleep in man a quantitative method of assessing baroreflex sensitivity. *Circulation Research*, 24(1):109–121, 1969.

[24] N Westerhof, J-W Lankhaar, and BE Westerhof. The arterial Windkessel. *Medical & Biological Engineering & Computing*, 47(2):131–141, 2009.

[25] F Yasuma and J Hayano. Respiratory sinus arrhythmia: why does the heartbeat synchronize with respiratory rhythm? *Chest Journal*, 125(2):683–690, 2004.